



Assessing the performance of the Lightning Imaging Sensor (LIS) using Deep Convective Clouds

Dennis E. Buechler ^{a,*}, William J. Koshak ^b, Hugh J. Christian ^a, Steven J. Goodman ^c

^a University of Alabama in Huntsville, Huntsville, AL, USA

^b Earth Science Office, ZP11, NASA Marshall Space Flight Center, Huntsville, AL, USA

^c National Oceanic and Atmospheric Administration (NOAA/NESDIS/GSFC), Greenbelt, MD, USA

ARTICLE INFO

Article history:

Received 14 February 2012

Received in revised form 21 September 2012

Accepted 25 September 2012

Keywords:

Lightning

LIS

Vicarious satellite calibration

Deep convective clouds

TRMM

GLM

ABSTRACT

The stability of the LIS instrument is examined during a 13 year period (1998–2010) by examining LIS background radiance observations of Deep Convective Clouds (DCCs) which are identified by their cold IR brightness temperature. Pixels in the LIS background image associated with DCCs are identified and analyzed during July and August of each year in the 13 year period. The resulting LIS DCC radiances are found to be stable throughout the period, varying at most by 0.8% from the 13 year mean July August value of $358.1 \text{ W sr}^{-1} \text{ m}^{-2} \mu\text{m}^{-1}$. The DCC method in this study provides a good approach for evaluating the stability of the future GOES-R Geostationary Lightning Mapper (GLM).

© 2012 Elsevier B.V. All rights reserved.

1. Introduction

The Lightning Imaging Sensor (LIS) onboard the Tropical Rainfall Measuring Mission (TRMM) satellite has been observing lightning activity over the Tropics since December 1997. Data collected from the LIS have been used in a number of studies involving lightning climatology, and for examining lightning characteristics of tropical convection (e.g., Albrecht et al., 2011; Cecil et al., 2013–this issue). It has been suggested that global tropical lightning trends with global warming (Williams 1992). However, due to longevity of the TRMM satellite in space (over 14 years), the question of instrument degradation and its effect on LIS flash detection efficiency becomes relevant. Changes in lightning detection efficiency can arise from a number of factors, including changes in calibration

due to aging, noise due to cosmic radiation or degradation of electronics. In addition to lightning parameters, the LIS also saves background (BG) data (described below) at a wavelength of 777.4 nm approximately every 35 min. LIS flash detection is related to the background radiance (Christian et al. 1989; Boccippio et al. 2002). Since 777.4 nm is within the solar reflective band, a vicarious calibration using Deep Convective Clouds (DCCs) as stable targets is applicable.

A number of studies using DCCs for satellite calibration and intercalibration for visible and near Infrared solar satellite data have been published (e.g. Doelling et al. 2004; Hu et al. 2004; Sohn et al., 2009). DCCs are used in these studies since they provide stable targets with consistent radiances. DCC pixels are identified by their cold infrared (IR) brightness temperatures and are then co-located to the solar reflective channel being analyzed. Here, we use the IR data from the Visible Infrared Sensor (VIRS, Kummerow et al. 1998) which is co-located with the LIS onboard the TRMM satellite. Brightness temperature observations from the VIRS 11 μm IR channel are used to identify DCCs for comparison with the LIS background radiance. DCCs are considered stable

* Corresponding author at: Earth System Science Center, University of Alabama in Huntsville, 320 Sparkman Drive, Huntsville, AL 35805, USA.

E-mail address: buechld@uah.edu (D.E. Buechler).

targets and the radiance contribution from the Earth's atmosphere is small compared to the solar reflectance off these very high clouds.

A method using DCCs is also being examined for potential use as a means of monitoring the performance of the future Geostationary Operational Environmental Satellite series R Geostationary Lightning Mapper (GOES-R GLM, Goodman et al., 2013). The GLM will be the first lightning detection system in geostationary orbit and will be able to detect total lightning (both intracloud and cloud-to-ground) during both day and night. Unlike low Earth-orbiting lightning sensors, GLM will be able to continually observe lightning activity within its field of view so that the evolution of lightning activity within thunderstorms can be monitored (Goodman et al., 2013). Fig. 1 illustrates the expected field of view of the GLM for both GOES-E and GOES-W positions. The current schedule has GOES-R being placed in the GOES-W position. The total lightning climatology shown in Fig. 1 was computed from observations by the Optical Transient Detector (OTD) (May 1995–March 2000) and the LIS (January 1998–December 2010) (Cecil et al., 2013–this issue).

The capability to continually track and monitor changes in total lightning activity within individual storms has the potential to improve forecasting of impending severe weather (Schultz et al. 2011). Thus it is important to be able to detect any changes in instrument calibration that may affect GLM's detection efficiency. Results from the current study using LIS data are relevant to GLM since they share a similar design.

2. The LIS measurement approach

The LIS consists of a 128×128 pixel charge-coupled device (CCD) that operates with a narrowband (0.909 nm width) interference filter in the solar reflective region of the spectrum at a wavelength of 777.4 nm, a wide field-of-view lens system, and a Real Time Event Processor (RTEP) (Christian et al. 1989; Koshak et al 2000). The 777.4 nm wavelength is used to optimize lightning detection since the lightning spectrum contains a prominent oxygen emission triplet near 777.4 nm.

As incident radiance is focused onto the pixel array, each pixel within the CCD array accumulates energy, integrating over frames of approximately 1.9 ms. Results are read out every 2 ms and passed to the RTEP. Since daytime solar illumination is much stronger than the lightning signal, a modified frame-by-frame background subtraction is implemented to remove the slowly varying background signal from the raw data coming off the LIS focal plane. The real-time processor continuously averages the output from the focal plane over six frames on a pixel-by-pixel basis in order to generate a background radiance estimate (BG). It then subtracts the BG from the current signal. When the difference between these signals exceeds a selected threshold, the signal is identified as a lightning event and is then transmitted to ground. Output from the entire BG array is also included in the ground data stream about every 35 s. During periods with very high event rates (either real lightning events or noise), LIS BGs and events can be lost due to data transmission limitations.

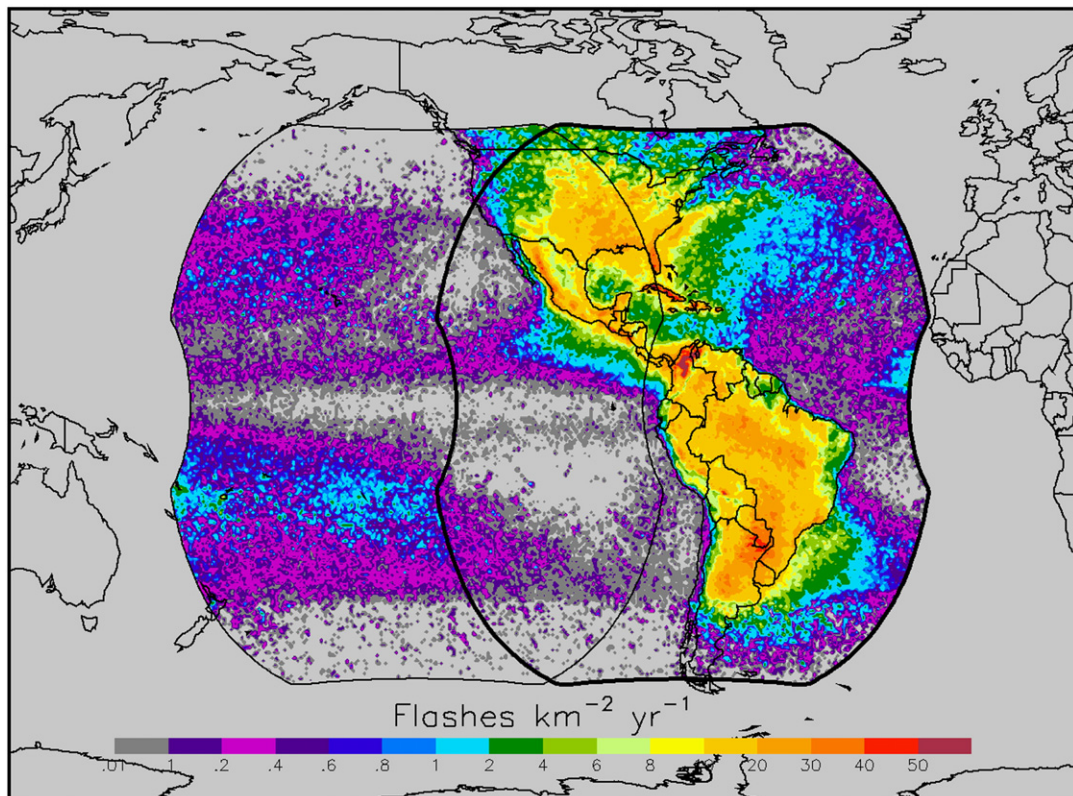


Fig. 1. Expected field-of-view of the Geostationary Lightning Mapper (GLM) from the east (bold outline) and west (thin outline) positions. The lightning statistics are derived from measurements from the LIS (January 1998–December 2010) and the Optical Transient Detector (OTD) (May 1995–March 2000) (Cecil et al., 2013–this issue).

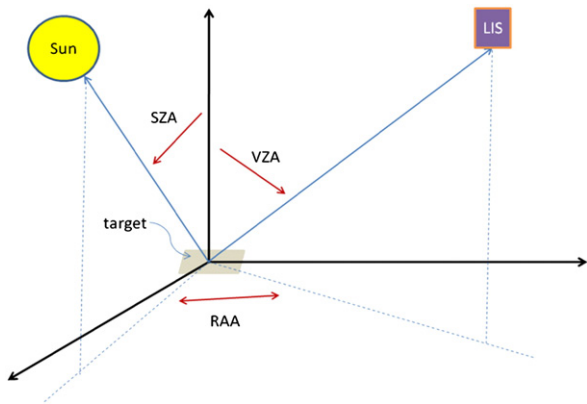


Fig. 2. Schematic of sensor and solar angles used in the DCC technique. The target is the location of a LIS pixel footprint. The Viewing Zenith Angle (VZA) is defined as the angle between LIS and a line perpendicular to the Earth's surface at the target. The Relative Azimuth Angle (RAA) is the angle between the Sun and the LIS vector projected onto a plane tangent to the Earth's surface. The Solar Azimuth Angle (SZA) is the angle between the Sun and a line perpendicular to the Earth's surface at the target.

This can occur during glint conditions or very active thunderstorm activity. High noise rates are also frequently encountered when the LIS is near the South Atlantic Anomaly (SAA) due to high energy particles impacting the CCD array.

Further processing is performed once the data have been transmitted to ground in order to filter out noise events. The events that remain are identified as lightning events and are then clustered into groups (similar to strokes), flashes, and areas (similar to thunderstorms). For further details on the LIS instrument design see Christian et al. (1989) and Christian et al. (2000).

3. Methodology

The methodology used here is similar to the Deep Convective Cloud Technique (DCCT) discussed by Hu et al. (2004) and Doelling et al. (2004). The DCCT identifies Deep Convective Clouds as cold bright earth targets. These clouds have been shown to have a consistent albedo over time with the peak in the albedo probability distribution near 0.75 with small variances (Hu et al. 2004), and they act as nearly Lambertian reflectors at low sun angles (Doelling et al. 2004). In addition, most of these clouds are near the tropopause level so that absorption and scattering effects between the satellite sensor and the DCC tops are minimal.

The data from both LIS and VIRS (co-located onboard the TRMM satellite) for each July and August from 1998 through 2010 were used to examine the LIS background radiance of DCCs. The TRMM satellite orbits at an inclination of 35°, from which it can monitor lightning activity between about 38° N and 38° S latitude. The satellite's altitude was 350 km from January 1998 until August 2001, when its orbit was boosted to 402.5 km to extend the lifetime of the mission. The nadir pixel resolution of LIS is 3.7 km pre-boost and 4.3 km post-boost, while the nadir resolution of VIRS is 2.2 km pre-boost and 2.4 km post-boost. A two-month period for each year was used to ensure a large sample size for the radiance distributions and to obtain coverage over the entire diurnal cycle. LIS BG data were converted from raw counts to

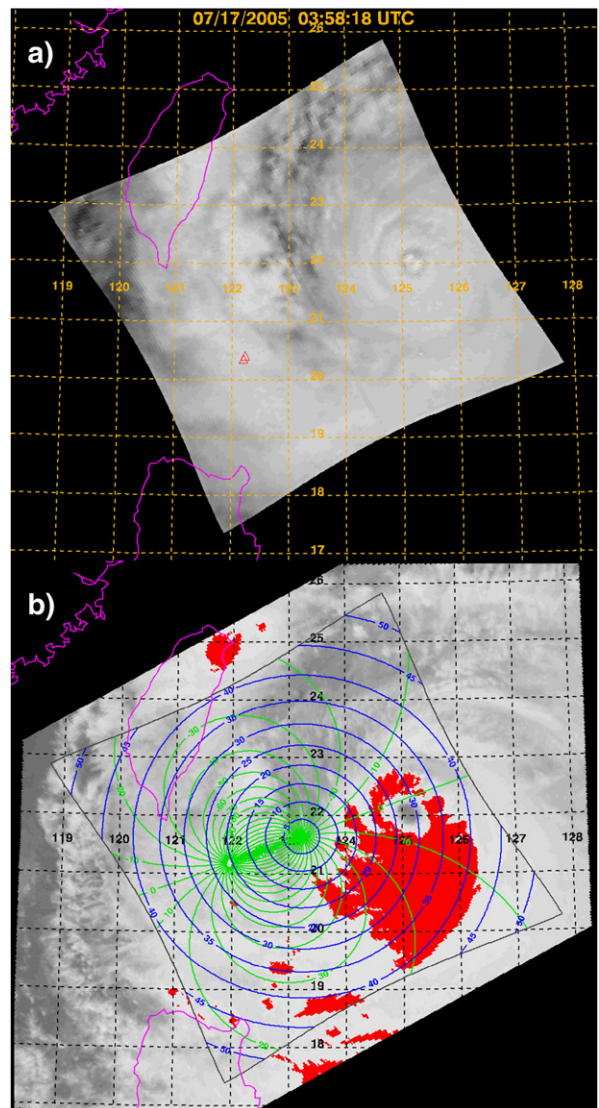


Fig. 3. Example of TRMM overpass of Super Typhoon Haitang on 17 July 2005 at 0358 UTC showing: a) the LIS BG radiance over its field of view as well as the location of 2 LIS-detected lightning flashes (red triangles), and b) the corresponding VIRS 11 μm Brightness Temperature image. The red shading indicates where T_b is less than 205 K. Contours of the LIS VZA (blue), RAA (green), and the LIS field of view coverage (gray) are also shown.

radiances using prelaunch calibration data (Koshak et al. 2000). The radiances were then adjusted as if they were observed from overhead by dividing by the cosine of the solar zenith angle (SZA). Hereafter, the term 'radiance' will be used to refer to the SZA adjusted value. An anisotropy factor (Loeb et al. 2003) is often applied to satellite radiance measurements to correct for effects due to SZA, VZA (Viewing Zenith Angle) and RAA (Relative Azimuth Angle) geometry (Fig. 2). We do not apply an anisotropy factor to the LIS BG radiance measurements since we are interested in the relative variation of observed radiance over time and the LIS DCC measurements are similarly distributed over SZA, VZA, and RAA during each July August period studied.

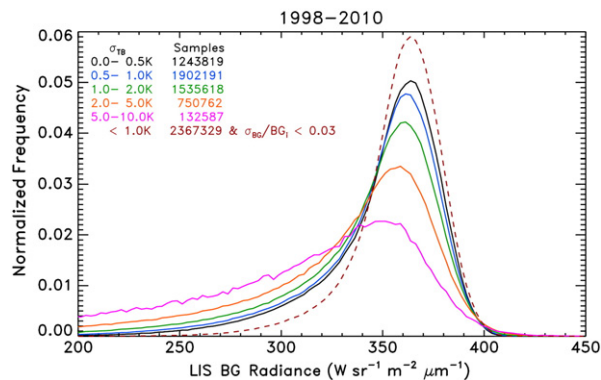


Fig. 4. Probability density functions of LIS BG radiance for July August 1998–2010 for LIS BG pixels co-located with VIRS pixels with $T_B < 205$ K. The solid lines show the LIS BG radiance distribution for pixels with $SZA < 40^\circ$, $10^\circ < RAA < 170^\circ$, and $VZA < 40^\circ$ for various ranges of σ_{TB} . The dashed red line is the LIS BG radiance probability function for pixels with the same angular constraints but where $\sigma_{TB} < 1$ K and $\sigma_{BG}/BG_i < 0.03$.

An example of a LIS BG image (Fig. 3a) and the corresponding image of VIRS $11 \mu\text{m}$ IR brightness temperature (T_B) (Fig. 3b) is shown during a TRMM overpass of Super Typhoon Haitang on 17 July 2005 at 3:58 UTC. Two lightning flashes (shown as red triangles in Fig. 3a) were detected during this overpass and they occur within the outer rain-band of the super typhoon. The cold cloud tops ($T_B < 205$ K) are shown in red (Fig. 3b) and occur near the center and within the rain-bands of Haitang. The LIS field of view is fully contained within that of the VIRS. Contours of VZA and RAA are also shown for illustration.

DCCs were identified within regions where the VIRS $11 \mu\text{m}$ T_B is less than 205 K. This brightness temperature threshold has been used in previous DCC studies (e.g., Hu et al. 2004; Doelling et al. 2004; Doelling et al. 2010). The locations of DCCs are constrained to $\pm 30^\circ$ latitude since the tropopause height is fairly consistent over that region (e.g., Seidel and Randel 2006) and DCC heights are near the tropopause. To ensure the DCC-identified pixel is within a spatially homogeneous cloud, a spatial homogeneity filter is applied. The filter uses the standard deviation of the brightness temperature of a given VIRS pixel and its 8 surrounding pixels (σ_{TB}). The LIS BG radiance distribution of co-located 205 K TB pixels (with angular constraints as described below) for various σ_{TB} thresholds are shown as solid lines in Fig. 4. The LIS BG radiance distributions become broader and the dark tail becomes more prominent as σ_{TB} increases. The dark tail of the distribution is due to cirrus that is optically thin at 777.4 nm and optically thick in the IR and is likely due to the spreading of cirrus anvils associated with the decaying stages of deep convection (Ham and Sohn, 2010; Doelling et al. 2010). A σ_{TB} threshold of 1 K is chosen to identify a DCC in order to minimize the dark tail, have a sharp radiance distribution and provide a sufficient number of DCC pixels for analysis.

Next, the LIS background pixels whose centers were closest to the IR identified DCC locations were selected for analysis. To reduce any effects associated with angular sampling, only LIS pixels that had the following constraints were used: SZA less than 40° , viewing zenith angle (VZA) less than 40° , and relative viewing angle (RAA) between 10° and 170° (see Fig. 2). Similar to the T_B data, a spatial homogeneity criterion is applied to the LIS BG pixels. The standard deviation of BG radiance of a given LIS pixel and its 8 surrounding pixels is obtained (σ_{BG}). Then

the ratio of σ_{BG} to the given LIS pixel radiance (BG_i) is computed (σ_{BG}/BG_i). The threshold value of this ratio for a pixel to be identified as a LIS BG DCC is set at 0.03. Further, LIS BG radiances can be contaminated by the occurrence of lightning since the sensor is optimized to detect lightning at this wavelength, so we use only pixels that have no lightning detected within 50 km of the pixel's center. The effect of no lightning and the σ_{BG}/BG_i criteria on the DCC radiance distribution can be seen in Fig. 4. The resulting distribution is sharper and the dark tail is further minimized while still retaining a large number of pixels for analysis. A summary of the LIS DCC criteria chosen for use in this study is shown in Table 1.

4. Results

Fig. 5 shows the geographical distribution of the LIS DCC pixels identified using the criteria in Table 1 and used in the analysis. It should be noted that LIS DCC occurrences are under sampled in and near the SAA due to limited background image availability in this region as noted earlier. The greatest concentrations of LIS DCCs are found in the Tropical Western Pacific, the East Indian Ocean and oceanic regions near Central America. Lesser oceanic LIS DCC concentrations are found within the Inter-Tropical Convergence Zone (ITCZ). Convection over land is limited, with only 7.4% of the LIS DCC pixels occurring over land. Due to the $SZA < 40^\circ$ and $VZA < 40^\circ$ criteria (Table 1), only DCCs that occur between 0900 and 1500 LT are analyzed. Since the area of cold cloud tops is still expanding over land at 1500 LT (Liu and Zipser 2008), relatively few IR pixels that have $\sigma_{TB} < 1$ are observed. In addition, lightning is

Table 1

Summary of DCC pixel criteria. The standard deviations (σ_{TB} , σ_{BG}) are computed from the values at the given pixel and the 8 surrounding pixels.

$T_B < 205$ K
$SZA < 40^\circ$
$VZA < 40^\circ$
$10^\circ < RAA < 170^\circ$
$\sigma_{TB} < 1$ K
$\sigma_{BG}/BG_i < 0.03$
No lightning within 50 km
All samples between 30 S and 30 N

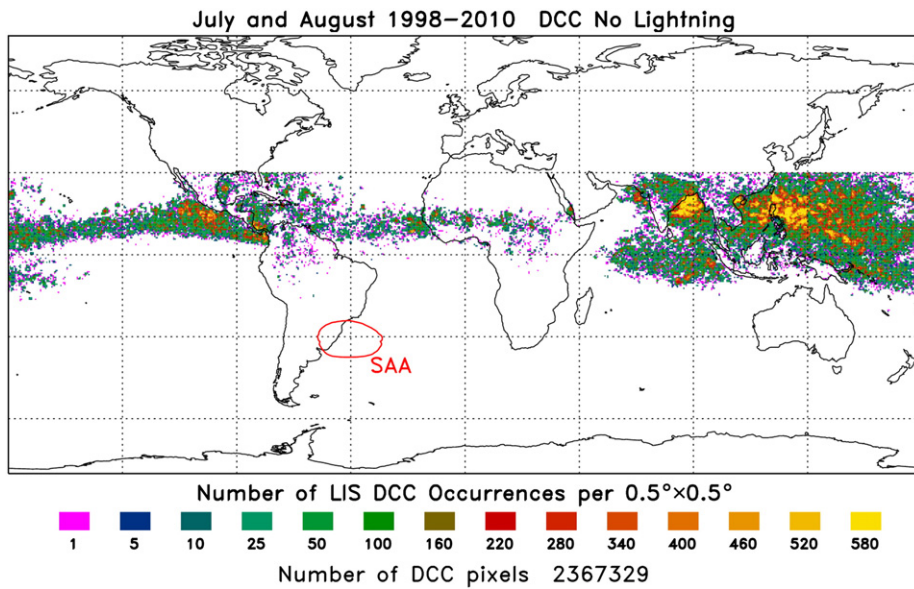


Fig. 5. Spatial distribution of the DCC pixels used in the analysis. The SAA is shown as the detection of LIS background images in and near this region is suppressed due to the high noise rate encountered here. The DCC pixels are constrained to $\pm 30^\circ$ latitude by definition (Table 1).

more prevalent with convection occurring over land (Christian et al. 2003; Liu and Zipser 2008), and by definition these pixels are not identified as LIS DCCs (Table 1). This spatial plot of DCC locations is consistent with that of July DCCs identified using data from the Moderate resolution Imaging Spectroradiometer (MODIS) by Doelling et al. (2010).

The LIS BG DCC radiances for each two monthly period (July and August) from 1998 to 2010 were binned into histograms with a bin size of $2.5 \text{ W sr}^{-1} \text{ m}^{-2} \mu\text{m}^{-1}$ (Fig. 6). The LIS DCC radiance distributions are very similar from one year to the next, indicating that the calibration has changed little if at all during the period. The time series of the mean LIS BG DCC for each July August period for each year is shown in Fig. 7. The solid line shows the July August DCC radiance for each year, while the dashed line is the mean of each of the 13 yearly July August values ($358.1 \text{ W sr}^{-1} \text{ m}^{-2} \mu\text{m}^{-1}$). The maximum

departure from the mean occurs during July August 2000 ($3.0 \text{ W sr}^{-1} \text{ m}^{-2} \mu\text{m}^{-1}$) and is a 0.8% departure from the mean. By comparison, Advanced Very High Resolution Radiometer (AVHRR) 0.86 and $0.65 \mu\text{m}$ channel DCC radiances exhibit degradation trends of 0.796%–3.5% per year, with a 3% variation of monthly values about the regression line (Doelling et al. 2004). In the current study, trends of a few years are observed, but no long term trend is apparent, indicating that the LIS calibration has been very stable throughout the years.

5. Summary and conclusions

The DCCT has been applied to data from LIS from 1998 to 2010. DCCs were identified through VIRS $11 \mu\text{m}$ channel brightness temperature observations. The co-located LIS BG pixels were then identified if they met certain criteria (Table 1). The radiances from the identified DCC LIS BG pixels were then analyzed. These included DCC from both land and oceanic locations.

This initial analysis of the DCC LIS BG radiances finds no apparent degradations of the instrument during the period from 1998 to 2010. The maximum yearly deviation in the mean DCC LIS BG radiance was 0.8% with no discernible trend over time. This indicates that LIS has been operating in a stable manner over its years in orbit. This is important for climatology work and other research examining variations in the lightning frequency.

This analysis bodes well for the GLM, which has a similar design to the LIS. The GLM will be operating in geostationary orbit so that space radiation effects will be greater than that experienced by the LIS. This could cause degradation of the instrument so it is important to monitor the GLM performance. The current results suggest that the DCCT would be an appropriate method. In the case of GLM, the IR cold cloud DCC pixels would be identified from IR channel measurements

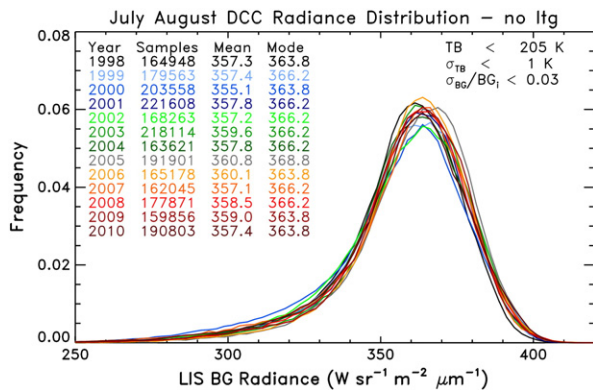


Fig. 6. Distribution of LIS BG DCC radiance for combined July and August for each year from 1998 to 2010. For each year, the number of DCCs identified (samples), as well as the mean and mode of the DCC radiance distribution are shown.

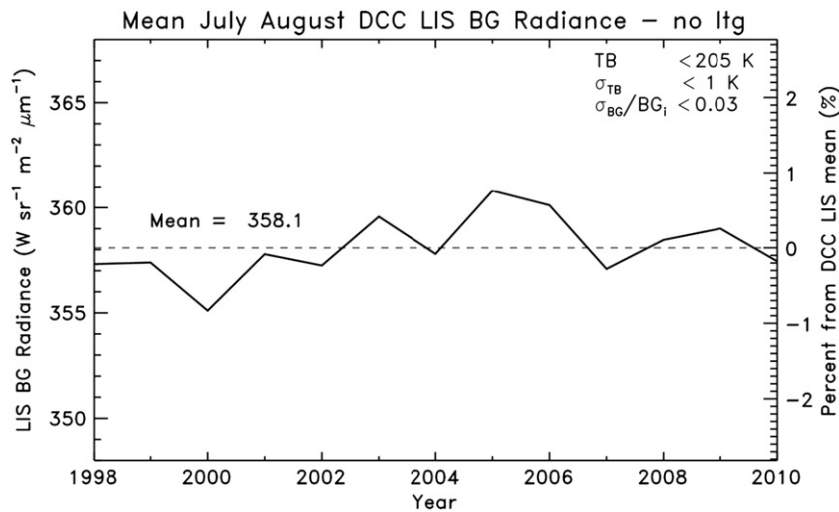


Fig. 7. Yearly values of mean LIS BG DCC radiance for each combined July and August from 1998 to 2010. The dashed line is the mean of each July August DCC radiance over the period ($358.1 \text{ W sr}^{-1} \text{ m}^{-2} \mu\text{m}^{-1}$). The left hand scale shows the mean in $\text{W sr}^{-1} \text{ m}^{-2} \mu\text{m}^{-1}$, while the scale on the right indicates the percentage departure from the mean July August 1998–2010 DCC radiance values.

available from the ABI (Advanced Baseline Imager) instrument also located on GOES-R (Schmit et al. 2005) and which will have onboard thermal channel blackbody calibration.

The DCCT for GLM would also work in the framework of the Global Space-Based Inter-Calibration System (GSICS, Goldberg et al. 2011), which aims to develop capabilities to intercalibrate geostationary satellite measurements using low earth sensors. Other groups are planning geostationary satellites with lightning detection instruments at different points around the earth. However, LIS would probably be gone by the time GOES-R is launched and there is no currently known low-earth replacement planned that could be used to intercalibrate the various geostationary lightning instruments.

Acknowledgments

This research has been supported by the NOAA GOES-R Calibration Working Group Program (managed by Changyong Cao) under Space Act Agreement # SAA8-061359, and by the Lightning Imaging Sensor (LIS) project (Program Manager, Ramesh Kakar, NASA Headquarters) as part of the NASA Earth Science Enterprise (ESE) Earth Observing system (EOS) project. We would also like to acknowledge the lightning team at NASA/MSFC who have supported LIS throughout the years. Thanks also to the reviewers of the paper (Themis Chronis, Earle Williams and an anonymous reviewer) for their comments and suggestions. LIS data is available from the NASA EOSDIS Global Hydrology Resource Center DAAC, Huntsville, AL, USA, <http://thunder.nsstc.nasa.gov>. The VIRS data was obtained from the GES DISC at: <http://mirador.gsfc.nasa.gov/index.shtml>.

References

Albrecht, R.I., Goodman, S.J., Petersen, W.A., Buechler, D.E., Bruning, E.C., Blakeslee, R.J., Christian, H.J., 2011. The 13 Years of TRMM Lightning Imaging Sensor: From Individual Flash Characteristics to Decadal Tendencies. XIV Int. Conf. Atmos. Elec. (Rio de Janeiro, Brazil).
Boccippio, D.J., Koshak, W.J., Blakeslee, R.J., 2002. Performance assessment of the Optical Transient Detector and Lightning Imaging Sensor,

Part I: predicted diurnal variation. *J. Atmos. Ocean. Technol.* 19, 1318–1332.
Cecil, D.J., Buechler, D.E., Blakeslee, R.J., 2013. Gridded Lightning Climatology from TRMM-LIS and OTD: Dataset Description. *Atmos. Res* 135–136, 401–411 (this issue).
Christian, H., Blakeslee, R., Goodman, S., 1989. The detection of lightning from geostationary orbit. *J. Geophys. Res.* 94, 13329–13337.
Christian, H.J., Blakeslee, R.J., Goodman, S.J., Mach, D.M., 2000. The Algorithm Theoretical Basis Document (ATBD) for the Lightning Imaging Sensor (LIS). Available from http://eospo.gsfc.nasa.gov/eos_homepage/for_scientists/atbd/docs/LIS/atbd-lis-01.pdf.
Christian, H.J., Blakeslee, R.J., Boccippio, D.J., Boeck, W.L., Buechler, D.E., Driscoll, K.T., Goodman, S.J., Hall, J.M., Mach, D.M., Stewart, M.F., 2003. Global frequency and distribution of lightning as observed from space by the Optical Transient Detector. *J. Geophys. Res.* 108. <http://dx.doi.org/10.1029/2002JD002347>.
Doelling, D.R., Nguyen, L., Minnis, P., 2004. On the use of deep convective clouds to calibrate AVHRR data. In: Barnes, W.L., Butler, J.J. (Eds.), *Earth Observing Systems IX Proc. SPIE Int. Soc. Opt. Eng.* 5542. <http://dx.doi.org/10.1117/12.560047>.
Doelling, D.R., Hong, G., Morstad, D., Bhatt, R., Gopalan, A., Xiong, X., 2010. The characterization of deep convective cloud albedo as a calibration target using MODIS reflectances. *Proc. SPIE Int. Soc. Opt. Eng.* 7862, 78620I. <http://dx.doi.org/10.1117/12.869577>.
Goldberg, M., Ohring, G., Butler, J., Cao, C., Datla, R., Doelling, D., Gartner, V., Hewison, T., Iacovazzi, B., Kim, D., Kurino, T., Lafeuille, J., Minnis, P., Renaut, D., Schmetz, J., Tobin, D., Wang, L., Weng, F., Wu, X., Yu, F., Zhang, P., Zhu, T., 2011. The Global Space-Based Inter-Calibration System. *Bull. Am. Meteorol. Soc.* 92, 467–475.
Goodman, S.J., Blakeslee, R.J., Koshak, W.J., Mach, D., Bailey, J.C., Carey, L.D., Buechler, D.E., Schultz, C.D., Bateman, M., McCaul, E., Stano, G., 2013. The GOES-R Geostationary Lightning Mapper (GLM). *Atmos. Res.* 125–126, 34–49.
Ham, S.-H., Sohn, B.J., 2010. Assessment of the calibration performance of satellite visible channels using cloud targets: application to Meteosat-8/9 and MTSAT-1R. *Atmos. Chem. Phys.* 10, 11131–11149. <http://dx.doi.org/10.5194/acp-10-11131-2010>.
Hu, Y., Wielicki, B.A., Yang, P., Stackhouse, P.W., Lin, B., Young, D., 2004. Application of deep convective cloud albedo observations to satellite-based study of terrestrial atmosphere: monitoring stability of spaceborne instruments and assessing absorption anomaly. *IEEE Trans. Geosci. Remote. Sens.* 42, 2594–2599.
Koshak, W.J., Stewart, M.F., Christian, H.J., Bergstrom, J.W., Hall, J.M., Solakiewicz, R.J., 2000. Laboratory calibration of the Optical Transient Detector and the Lightning Imaging Sensor. *J. Atmos. Oceanic Technol.* 17, 905–915.
Kummerow, Christian, Barnes, William, Kozu, Toshiaki, Shiue, James, Simpson, Joanne, 1998. The Tropical Rainfall Measuring Mission (TRMM) sensor package. *J. Atmos. Ocean. Technol.* 15, 809–817.
Liu, C., Zipser, E.J., 2008. Diurnal cycles of precipitation, clouds, and lightning in the tropics from 9 years of TRMM observations. *Geophys. Res. Lett.* 35, L04819. <http://dx.doi.org/10.1029/2007GL032437>.

- Loeb, N.G., Manalo-Smith, N., Kato, S., Miller, W.F., Gupta, S.K., Minnis, P., Wielicki, B.A., 2003. Angular distribution models for top-of-atmosphere radiative flux estimation from the Clouds and the Earth's Radiant Energy System instrument on the Tropical Rainfall Measuring Mission satellite. Part 1: methodology. *J. Appl. Meteorol.* 42, 240–265.
- Schmit, T.J., Gunshor, M.M., Menzel, W.P., Gurka, J.J., Li, J., Bachmeier, A.S., 2005. Introducing the next-generation Advanced Baseline Imager on GOES-R. *Bull. Am. Meteorol. Soc.* 86, 1079–1096.
- Schultz, Christopher J., Petersen, Walter A., Carey, Lawrence D., 2011. Lightning and severe weather: a comparison between total and cloud-to-ground lightning trends. *Weather Forecast.* 26, 744–755.
- Seidel, D.J., Randel, W.J., 2006. Variability and trends in the global tropopause estimated from radiosonde data. *J. Geophys. Res.* 111, D21101. <http://dx.doi.org/10.1029/2006JD007363>.
- Sohn, B.-J., Ham, S.-H., Yang, P., 2009. Possibility of visible-channel calibration using deep convective clouds overshooting the TTL. *J. Appl. Meteorol. Climatol.* 48, 2271–2283.
- Williams, E.R., 1992. The Schumann resonance – a global tropical thermometer. *Science* 256, 1184–1187.